research articles Journal of proteome research

Integrated Cytokine and Metabolic Analysis of Pathological Responses to Parasite Exposure in Rodents

Jasmina Saric,[†,⊥] Jia V. Li,[†,⊥] Jonathan R. Swann,[†] Jürg Utzinger,[‡] Gail Calvert,[§] Jeremy K. Nicholson,[†] Stephan Dirnhofer,[#] Maggie J. Dallman,[||] Magda Bictash,[*,†] and Elaine Holmes[*,†]

Biomolecular Medicine, Department of Surgery and Cancer, Faculty of Medicine, Imperial College London, Sir Alexander Fleming Building, South Kensington, London SW7 2AZ, United Kingdom, Department of Public Health and Epidemiology, Swiss Tropical Institute, P. O. Box, CH-4002 Basel, Switzerland, Meso Scale Discovery, 9238 Gaither Road, Gaithersburg, Maryland 20877, Institute of Pathology, University Hospital Basel, CH-4031 Basel, Switzerland, and Faculty of Natural Sciences, Imperial College London, Sir Alexander Fleming Building, South Kensington, London SW7 2AZ, United Kingdom

Received November 9, 2009

Parasitic infections cause a myriad of responses in their mammalian hosts, on immune as well as on metabolic level. A multiplex panel of cytokines and metabolites derived from four parasite-rodent models, namely, *Plasmodium berghei*—mouse, *Trypanosoma brucei brucei*—mouse, *Schistosoma mansoni*—mouse, and *Fasciola hepatica*—rat were statistically coanalyzed. ^{1}H NMR spectroscopy and multivariate statistical analysis were used to characterize the urine and plasma metabolite profiles in infected and noninfected animals. Each parasite generated a unique metabolic signature in the host. Plasma cytokine concentrations were obtained using the 'Meso Scale Discovery' multi cytokine assay platform. Multivariate data integration methods were subsequently used to elucidate the component of the metabolic signature which is associated with inflammation and to determine specific metabolic correlates with parasite-induced changes in plasma cytokine levels. For example, the relative levels of acetyl glycoproteins extracted from the plasma metabolite profile in the *P. berghei*-infected mice were statistically correlated with IFN-γ, whereas the same cytokine was anticorrelated with glucose levels. Both the metabolic and the cytokine data showed a similar spatial distribution in principal component analysis scores plots constructed for the combined murine data, with samples from all infected animals clustering according to the parasite species and whereby the protozoan infections (*P. berghei and T. b. brucei*) grouped separately from the helminth infection (*S. mansoni*). For *S. mansoni*, the main infection-responsive cytokines were IL-4 and IL-5, which covaried with lactate, choline, and D-3-hydroxybutyrate. This study demonstrates that the inherently differential immune response to single- and multicellular parasites not only manifests in the cytokine expression, but also consequently imprints on the metabolic signature, and calls for in-depth analysis to further explore direct links between immune features and biochemical pathways.

Keywords: Metabolic Profiling • *Plasmodium berghei* • *Trypanosoma brucei brucei* • *Fasciola hepatica* • *Schistosoma mansoni* • Cytokine Patterns • Systems Integration • ^{1}H NMR Spectroscopy • Multivariate Data Analysis

Introduction

Parasitic infections induce a variety of biochemical responses in the host, including modulation of energy metabolism,[1−3] inflammation,[4−6] anemia,[7−9] and nutrient deficiencies.[10−12] The effective control and eventual elimination of these invading organisms is generally mediated by both cellular and humoral immune mechanisms, and includes different T cell-effector mechanisms, such as those reflected by the increase in Th1, Th17, Th2 subtype CD4$^+$ cells, as well as regulatory T-cells.[13−19] The Th1/Th2 paradigm originally postulated by Mosmann and Coffman in 1986 described a framework for understanding immunological control mechanisms,[20] which were simplified into two main mechanisms: Th1 or 'cell-mediated' immunity and Th2 or 'humoral' immunity. Intracellular parasites (e.g., bacteria and protozoa) are effectively fought by a Th1 response and the promotion of direct cytotoxic activity, which, in turn, can lead to tissue damage in the host.[6,19] Helminth infections, in contrast, are controlled by Th2-based immune mechanisms, which involve secretion of antibodies, promotion of eosino-

* To whom correspondence should be addressed. Magda Bictash, Biomolecular Medicine, Department of Surgery and Cancer, Faculty of Medicine, Imperial College London, Sir Alexander Fleming Building, South Kensington, London SW7 2AZ, United Kingdom. Tel., +44 20 7594-3230; fax, +44 20 7595-3220; e-mail, magda.bictash@imperial.ac.uk. Elaine Holmes, Biomolecular Medicine, Department of Surgery and Cancer, Faculty of Medicine, Imperial College London, Sir Alexander Fleming Building, South Kensington, London SW7 2AZ, United Kingdom. Tel., +44 20 7594-3220; fax, +44 20 7595-3220; e-mail: elaine.holmes@imperial.ac.uk.

† Department of Biomolecular Medicine, Imperial College London.

⊥ These authors contributed equally to the work reported here.

‡ Swiss Tropical Institute.

§ Meso Scale Discovery.

University Hospital Basel.

|| Faculty of Natural Sciences, Imperial College London.

10.1021/pr901019z

Published on Web 01/22/2010

philia (IL-5),[21] production of IgE and IgG1 (IL-4), mastocytosis, and mediation of helminth expulsion.[22,23]

However, this original Th1/Th2 dogma is somewhat oversimplified and it is necessary to consider emerging evidence of other immunological processes. For example, Th17 subtype $CD4^+$ cells, which are reported to control microparasites effectively (e.g., bacteria and fungi) also promote certain autoimmune mechanisms,[17,24,25] whereas T-regulatory cells (Tregs) are activated in an exclusive fashion to Th17 cells and fine-tune the immune-response of the host.[14−16]

The immune outcome and the associated cytokine profile manifested by the host in response to parasitic infection are dependent upon the parasitic species, intensity of infection, the first organ of antigen exposure and also the cytokine milieu already present within the host.[26]

In addition to immunologic changes, parasitic infections cause direct cellular events such as altered energy metabolism. Metabolic profiling strategies combining spectroscopic fingerprinting with mathematical modeling have previously been applied to characterize the global response of the host at the metabolic level and have been discussed in the light of specific measured inflammatory components in particular disease conditions, such as breast cancer[27] and colitis,[28] but thus far metabolic signatures of pathology have not been systematically modeled with immunological profiles.

Several single-parasite infection models have been investigated in rodents, using ^{1}H nuclear magnetic resonance (NMR) spectroscopy to generate biochemical signatures of various biological fluids and tissues. These studies have defined panels of metabolic biomarkers reflective of the various components of the biological response to specific parasites. In addition to biochemical changes induced as a direct consequence of tissue pathology, some components of these metabolic responses are likely to be directly linked to immunologic events, in particular the inflammatory response. For example, a *Trypanosoma brucei brucei* infection in the mouse has been associated with increased circulating levels of acetylated glycoproteins,[29] which are normally secreted in the liver in response to pro-inflammatory cytokines. Conversely, increased plasma levels of lactate and depleted glucose have also been documented to be a feature of a *T. b. brucei* infection in the mouse and imply increased glycolytic activity in the parasite independent of the inflammation.[29]

Here, we assess covariance between immunological parameters as defined by the pattern of multiple cytokines, and the metabolic phenotypes, as defined by the ^{1}H NMR spectral profiles, in biofluids obtained from four parasite−rodent models. We propose a new strategy for correlating the plasma concentrations of several selected Th1/Th2 cytokines with the biochemical signature of the different parasite−rodent models, including protozoan (Th1-inducing) and helminth (Th2-inducing) infections and elucidate model-dependent and model-independent associations of inflammatory measures with metabolic phenotypes with a view to highlighting the component of the metabolic signature, which is associated with, or modulated by, parasite-specific host inflammatory responses.

Methods

The levels of selected plasma cytokines were coanalyzed with pre-existing spectroscopic data from four different parasite−rodent models.

Animal Husbandry and Sample Collection. All animal experiments were carried out at the Swiss Tropical Institute (Basel, Switzerland) and complied with Swiss local and national regulations on animal welfare (permission no. 2081). Three separate batches of NMRI female mice were purchased from RCC (Itingen, Switzerland). Animals were kept under environmentally controlled conditions (light/dark cycle, 12/12 h; temperature, ∼22 °C; relative humidity, 60−70%) with unrestricted access to community tap water and standard rodent diet (NAFAG; Gossau, Switzerland). Animals were acclimatized for 1−2 weeks prior to the onset of each experiment. Sample collection in the *Plasmodium berghei*−mouse, *T. b. brucei*−mouse and *Schistosoma mansoni*−mouse models have been described elsewhere.,[2,3,30] In brief, urine samples were collected into a Petri dish by gently rubing the abdomen until a minimum volume of 20 μL was obtained. Whole blood was collected from the tail tip of the mice using sodium heparin-coated hematocrit capillaries. The plasma was separated from the cellular components by centrifuging the whole blood sample at 4,000 *g* for 4 min. Both urine and plasma samples were transferred into Eppendorf tubes on dry ice immediately after collection prior to storage at −40 °C.

Additionally, a *Fasciola hepatica*−rat model was included, which allowed subsequent comparison between results obtained from mice and rats. The experimental details from each of the parasite−rodent models are summarized in Table 1 and a reference provided to indicate the rationale for selection of the infection intensities and sampling time points for each model.[31−34]

For the cytokine analysis, 5 infected and 5 noninfected control animals were analyzed for the *T. b. brucei*−mouse model (28 days postinfection), and 5 infected and 4 noninfected control animals for the *F. hepatica*−rat model (22 days postinfection). In the case of *S. mansoni*−mouse (53 days postinfection), 7 infected and 5 noninfected animals were used due to the observed variation in metabolic profiles in the infected group. Since the duration of the *P. berghei* model was only 4 days, an age-matched control group was deemed unnecessary, particularly in view of the 3R rules (reduce, replace, and refine), and hence the postinfection samples group (day 4) was directly compared with the preinfection samples group.

^{1}H NMR Spectroscopy of Urine and Plasma Samples. Urine and plasma samples were analyzed using standard one-dimensional (1D) ^{1}H NMR spectroscopy at 600 MHz with suppression of the water signal, according to a published protocol.[30]

Quantitative Cytokine Level Measurement in Plasma Samples. Cytokine measurements were made using the 'Meso Scale Discovery' (MSD)-based multi cytokine approach.[34] The commercial mouse-specific 96-well multispot plate of Th1/Th2 cytokines (TNF-α, mKC, IL-5, IL-4, IL-2, IL-1β, IL-12, IL-10, and IFN-γ) was used for the murine models and the corresponding rat demonstration kit (IFN-γ, IL-1β, IL-4, IL-5, IL-13, KC/GRO, and TNF-α) was selected for the *F. hepatica*−rat model. The concentrations of cytokines were quantified using an 8-point calibration curve constructed from a plot of the signal intensity for a series of known concentrations of the multiplex standard provided by the kit manufacturer. The data were analyzed using MSD Workbench software and the curves fitted using the built-in 4PL fit with $1/y^2$ weighting ($y = b_2 + ((b_1 - b_2)/(1 + (x/b_3)^{b4}))$. Validation of the MSD platform and comparison with Luminex, a different multiplex technology has been conducted previously.[35]

Each plasma sample was measured in duplicate and an aliquot of 20 μL placed into separate wells. The measurement

Table 1. Infection Parameters of the 4 Parasite-Rodent Models Employed

Parasite and reference source	Host	No. animals[a]	Infection intensity	PCV at last sampling timepoint	Main histo-pathological features	Time of sampling	Altered cytokines[b]	Main metabolic changes in urine	Main metabolic changes in plasma
Plasmodium berghei [3,31]	NMRI ♀ mice	n(P)=5 n(T)=5	Infected RBC: 34.4% SD: 5.2	C=55.0% T=33.0%	Reactive follicular hyperplasia in the spleen	Days -1, 4	↑ *IL-12 ↑ *MKC ↑ IFN-γ ↑ IL-4	↑ dimethylamine ↓ trimethylamine-*N*-oxide ↑ phenylacetylglycine ↓ taurine ↑ pipecolic acid ↑ 2-oxoisovalerate	↓ acetate ↓ creatine ↓ glycerophosphocholine ↑ lactate ↑ pyruvate ↓ glucose
Trypanosoma brucei brucei [30,32]	NMRI ♀ mice	n(C)=5 n(T)=5	164,000 trypanosomes per μl blood	no information	Hemopoiesis in the liver and renal interstitial nephritis	Day 28	↑ IL-1β ↑ IL-5 ↑ *IL-12 ↑ IFN-γ	↑ lactate ↑ trimethylamine ↑ tryptophan ↑ 4-hydroxyphenylacetic acid ↓ hippurate ↑ 2-oxoisovalerate	↑ lactate ↓ glucose ↓ leucine ↑ *O*-acetyl glycoprotein ↑ choline ↑ creatinine
Schistosoma mansoni [33]	NMRI ♀ mice	n(C)=5 n(T)=7	AWB: 36 Range: 26-46 SD: 7	C=54.7% T=33.7%	Lymphfollicular hyperplasia in the spleen	Day 53	↑ IL-4 ↑ IL-5 ↑ *IL-12 ↑ IFN-γ	↓ 2-oxoisocaproate ↑ trimethylamine ↓ 2-oxoadipate ↑ phenylacetylglycine ↓ hippurate ↑ 3-ureidopropionate	↓ creatine ↓ D-3-hydroxybutyrate ↓ acetate ↓ glucose ↓ citrate ↑ triglycerides
Fasciola hepatica [34]	Wistar ♀ rats	n(C)=4 n(T)=5	AWB: 5.5 Range: 2-10 SD: 3.8	C=50.8% T=42.0%	Necrotic parenchymal changes in the liver, splenic follicular hyperplasia and inflammatory infiltrates in the kidney	Day 22	↑ IL-1β ↑ IL-5 ↑ **IL-13 ↓ IFN-γ	↓ creatinine ↓ taurine ↑ bile acid	↓ triglycerides ↓ TMAO ↑ leucine ↑ isoleucine ↑ valine ↑ acetyl glycoproteins

[a] No. animals: (C), non-infected animals; (T), infected animals; and (P), pre-infection; ↑ increased upon infection, ↓ decreased upon infection. Altered Cytokines: Top 4 cytokines that co-map with the infection in the PCA analysis. *Specific for mouse and **Specific for rat multi-cytokine panel.

procedure was performed according to the manufacturer's protocol with the exception that the incubation time used was 4 h. Plasma samples from all selected animals were obtained after nondestructive ^{1}H NMR spectral acquisition (e.g., a 1:1 dilution in saline, containing 90% deuterated water, was implemented); hence, the incubation time was extended from 2 to 4 h in order to compensate for the dilution factor and to increase the sensitivity of the assay. A MSD Sector Imager (Sector Imager 6000; Gaithersburg, MD) was utilized to read the plates.

Multivariate Statistical Data Analysis. Principal component analysis (PCA) was applied to each individual parasite−host data set and also to the combined murine data for *S. mansoni*, *P. berghei*, and *T. b. brucei* infections. Since PCA is an unsupervised method and makes no assumption as to the origin or class of samples, it allows the major sources of variance in a data set to be defined without incorporating inherent bias. Application to a complex matrix, such as those represented here by the NMR spectral data or the cytokine data (*X*-matrix), achieves a reduction in the dimensionality of the data matrix, identifies outliers and facilitates visualization of the data distribution.[36,37]

To maximize the variance in the NMR data related to the response to the infection, supervised multivariate methods were also applied. Projection to latent structure discriminant analysis (PLS-DA) was conducted on both the NMR data and the cytokine data separately, using a binary code to indicate infection or noninfection as the *Y*-matrix. The information on class membership allows optimal extraction of the particular observations (e.g., metabolites), which are responsible for the differentiation of groups and can maximize separation in the PLS-DA model. However, PLS-DA can also include variation that is not response class or *Y*-related. By incorporation of an orthogonal filter (O-PLS), systematic variation unrelated to infection status can be removed and thereby facilitates the interpretation of infection-related effects.[38] Here, an in-house adapted O-PLS script was used[39] to perform a cross-matrix correlation between ^{1}H NMR-derived spectral information (*X*) and identity matched single cytokine levels (*Y*) in order to find connections between metabolic and immune metrics.

Results

Physiological Monitoring of Rodents over the Course of Infection. The establishment of infection in the 4 parasite−rodent models employed was verified by hematologic parameters and histological examination. Worm counts upon dissection were also used in the case of helminths. All parasitic infections induced clear pathology in all infected animals as described in Table 1, with the exception of the *S. mansoni*−mouse model, where the establishment of infection could not be confirmed for 2 out of 7 infected mice. Images of hematoxylin and eosin stained selected sections of host organs are provided for each of the four infection models in Figure 1, showing pathological events in spleen tissue sections from *P. berghei* (Figure 1A) and *S. mansoni*-infected mice (Figure 1C) and in liver sections from *F. hepatica*-infected rats (Figure 1B), and *T. b. brucei*-infected mice (Figure 1D). Pathological changes were also observed in the kidney of *T. b. brucei*-infected mice,[30] which showed interstitial nephritis and *F. hepatica*-infected rats demonstrated splenic follicular hyperplasia with inflammatory infiltrates found in the kidney (unpublished data) (Table 1).

Metabolic Characterization of Parasite Effects in Rodent Models. The parasite-infected animals were easily differentiated from noninfected controls using PCA and O-PLS-DA models and the disease-related biological markers were extracted from urinary and plasma metabolite profiles.

Metabolic characterization of the *T. b. brucei*−mouse,[30] and *P. berghei*−mouse[3] models has been conducted and described previously. In brief, the infection with both protozoan parasites induced depleted plasma glucose concentrations and subsequently increased lactate levels, reflecting a higher glycolytic activity postinfection. Increased levels of *O*-acetyl glycoproteins were found in the plasma of *T. b. brucei*, but not *P. berghei*-

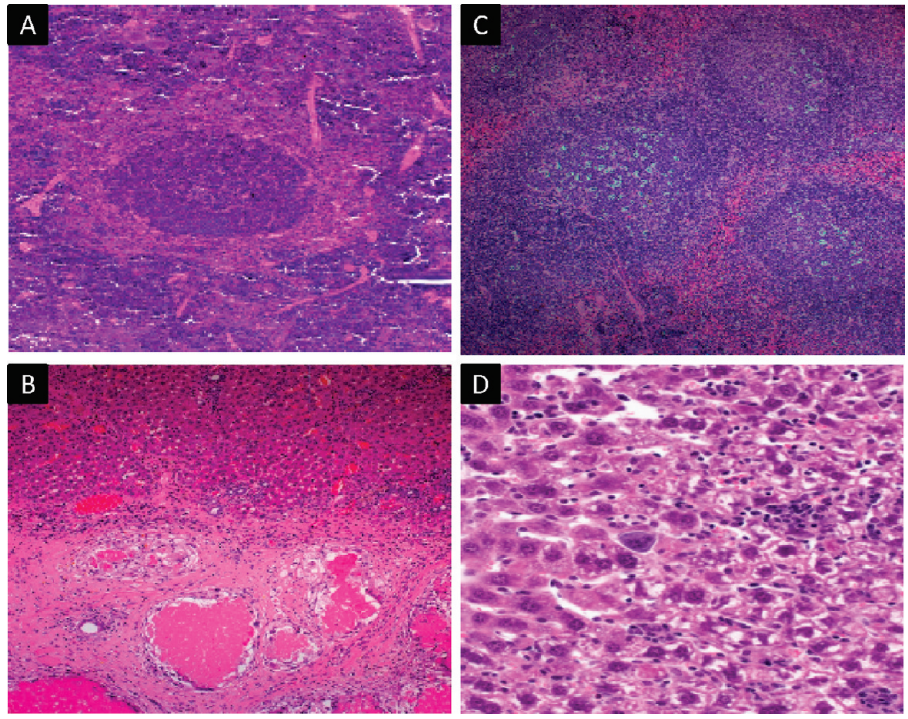

Figure 1. (A) Reactive follicular hyperplasia detected in a mouse spleen 4 days after infection with *P. berghei*. Large germinal centers are shown, formed of immune- and centroblasts. Red pulp congestion was further indicated by abundant hemozoin in cordal macrophages; (B) liver tissue sections from a *F. hepatica*-infected rat showing typical cavity-like necrotic tunnels that were demarked by a foreign body reaction (100×); (C) lymphofollicular hyperplasia was detected in the spleen of *S. mansoni*-infected mice and indicated by prominent germinal centers including tangible body macrophages; (D) hepatic hemopoiesis after infection with *T. b. brucei*.

infected mice. The urinary manifestation of both protozoan species shared some similarities, including an increase in 2-oxoisovalerate levels, but also elicited disease specific markers, such as increased pipecolic acid (*P. berghei*) and increased 4-hydroxyphenyl acetic acid (*T. b. brucei*).

F. hepatica induced systematic changes in the plasma metabolite profile as illustrated in the O-PLS-DA coefficient plot (Figure 2A). *F. hepatica* infection caused a decrease in plasma levels of TMAO, and increased relative levels of the *O*- and *N*-acetyl glycoproteins (Figure 2A), with a concomitant depletion of urinary creatinine and taurine. A relative increase in the concentration of bile acids was also evident. The scores from both the O-PLS-DA and the PCA models constructed from the plasma ^{1}H NMR spectral data of *F. hepatica*-infected rats on day 22 postinfection, when overt pathology was established, demonstrated discrete clustering of ^{1}H NMR plasma spectra relating to control and infected rats (Figure 2B) (O-PLS-DA: $R^2Y = 0.90$, $Q^2Y = 0.57$; PCA: $R^2_{cum}X = 0.96$, $Q^2X = 0.40$). One O-PLS component and one orthogonal component were used for the O-PLS-DA model, whereas for the PCA analysis three principal components (PCs) were used to construct the model.

Global PCA and PLS-DA analyses on the combined spectral data sets derived from the three murine models showed that the samples from the protozoan infections were biochemically distinct from samples from *S. mansoni*-infected mice, which formed a separate cluster along the axis of the third PC (Figure 3A and Supporting Information). The PLS-DA model was constructed using three PCs (PLS-DA: $R^2X = 0.40$, $R^2Y = 0.71$, $Q^2Y = 0.33$). From the scores and the corresponding loadings, it was apparent that the biochemical composition of the control samples relating to each parasite−host model differed according to batch, particularly with respect to *T. b. brucei*. These observed batch differences are unsurprising given that an outbred mouse strain was used as the host. Furthermore, age-dependent variation might contribute to the differences within the control groups; all control animals were approximately the same age prior to the infection, but due to the different length of time required to establish a patent infection, the time of sampling ranged from 4 days postinfection in the shortest model (*P. berghei*) to 53 days postinfection in the longest (*S. mansoni*). However, despite the interbatch variation, it was obvious that the *S. mansoni* infection drove the metabolite profiles in a different direction to the two protozoan infections and that the batch differences could be largely eliminated by use of O-PLS modeling (data not shown).

The recovery of urine and plasma metabolic candidate biomarkers (1D standard pulse program) for *S. mansoni via* O-PLS-DA comprised higher levels of urinary phenylacetylglycine and 3-ureidopropanoate, and lower relative levels of 2-oxoisocaproate, hippurate and 2-oxoiadipate, while the plasma profile was characterized by lower concentrations of acetate, glucose and citrate, but relatively higher lipoprotein fractions (Table 1). The spectral PCA scores plot of plasma samples from *S. mansoni*-infected and noninfected mice showed three separate groupings (Figure 4A), whereby in addition to clear separation of infected and noninfected animals, a third cluster was evident, consisting of two individual mice that underwent initial infection but where infection failed to establish, as evidenced by zero worm counts upon dissection of these mice. The PLS-DA model was built using two components (PLS-DA: $R^2X = 0.32$, $R^2Y = 0.83$, $Q^2Y = 0.20$).

Characterization of the Immune Response to Parasite Infection Using Multiplex Cytokine Assays. Separate PLS-DA models were constructed comparing infected and noninfected

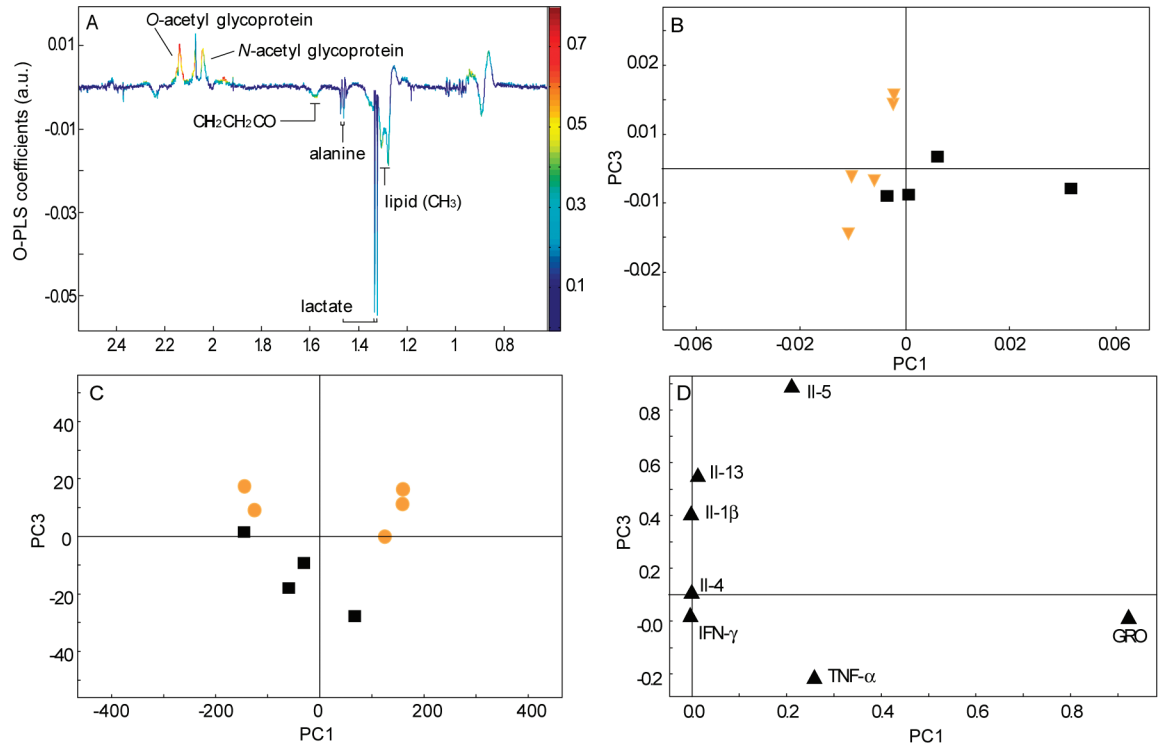

Figure 2. Differentiation of plasma samples obtained from a pairwise comparison of plasma ^{1}H NMR data of *F. hepatica*-infected *vs.* noninfected control rats at day 22 postinfection. (A) O-PLS-DA coefficient plot; (B) PCA of ^{1}H NMR plasma data; (C) PCA scores plot; and (D) PCA coefficients plot based on the relative levels of selected cytokines assessed on day 22 postinfection in *F. hepatica*-infected rats (orange) and noninfected control rats (black).

control animals for each parasite−rodent model, or in the case of *P. berghei*, pre- and postinfection status. The top 4 discriminating variables (i.e., cytokines) were extracted. For *P. berghei* infection, IL-12, mKC, IFN-γ, and IL-4 were the 4 most discriminatory cytokines between the pre- and postinfection time points, whereas the *T. b. brucei*-infected mice were discriminated from the controls at day 28 postinfection mainly by IL-1β and IL-5. The main discriminatory cytokines for each pairwise comparison of infection and noninfection status investigated are listed in Table 1. The cytokine distribution of rats infected with *F. hepatica* was also clearly differentiated from that of controls as shown in the PCA scores and loadings plots (Figures 2C,D), whereby separation was mainly influenced by increased IL-5 levels in infected animals ($R^2_{cum}X = 0.99$, $Q^2X = 0.71$). Three PCs were used to build the model. Similarly to the analysis of the metabolic data, PCA analysis of cytokine data of the *S. mansoni*-infection model indicated the presence of three different groups, one of which corresponded to the two animals in the infected group in which infection failed to establish (Figures 4C,D) ($R^2_{cum}X = 0.67$, $Q^2X = 0.25$). The model was constructed using 2 PCs. Samples from these animals were clearly separated from both uninfected controls and the infected mice, and the mapping position from these anomalous mice was mainly influenced by the plasma level of mKC, which was relatively higher in these two mice than in either the infected or the noninfected control animals (Figures 4C,D).

To compare plasma levels of the cytokines across the different parasitic infections in the same host species (i.e., NMRI mouse), PCA analyses were carried out on the integrated murine data set using two PCs ($R^2_{cum}X = 0.67$, $Q^2X = 0.18$). The distribution of the samples in a multivariate space was compared for the three murine infection models based on the cytokine composition (Figure 3C,D), as determined *via* the PCA scores and loadings plots (*S. mansoni* on day 53 postinfection, *T. b. brucei* on day 28 postinfection, *P. berghei* on day 4 postinfection). The two protozoan infections demonstrated a similar trend in mapping position in the plots and deviated from the control group in the first PC, but *T. b. brucei*-infected mice had a wider spread compared to the animals infected with *P. berghei*, indicating greater variation in response to infection. In contrast, the trematode *S. mansoni* induced an orthogonal shift in the second PC direction compared to the two protozoan infections, with a marked discrimination from the controls also along the second PC axis. Higher levels of IL-4 and IL-5 dominated the separation between *S. mansoni*-infected animals from both protozoan infected and noninfected control mice. Increased concentrations of IL-12, TNF-α, IL-10, IFN-γ, and IL-2 were the main contributors to the discrimination of the mice infected with protozoa.

Inter-Matrix Data Correlation of Relative Cytokine Levels and ^{1}H NMR Spectral Intensities. The matrices for both the NMR-characterized metabolite profiles and the cytokine data were statistically related using O-PLS analysis in order to obtain information on potentially causal events at the interface of the metabolic and immune systems. The model was constructed using one PLS component and one orthogonal component (O-PLS-DA: $R^2Y = 0.99$, $Q^2Y = 0.77$). There were several statistically significant correlations between the relative cytokine levels and the corresponding plasma spectra of 5 mice preinfection and at days 2 and 4 postinfection in mice infected with *P. berghei* (Figure 5). A positive correlation was found between IFN-γ and plasma concentrations of *N*-acetyl glycoprotein fragments, lactate, creatine, and glycine, whereas IFN-γ was anticorrelated with glucose. The same correlation script was applied to urine and plasma spectra from each of the parasite−host models. Although trends in covariation between metabolites and cy-

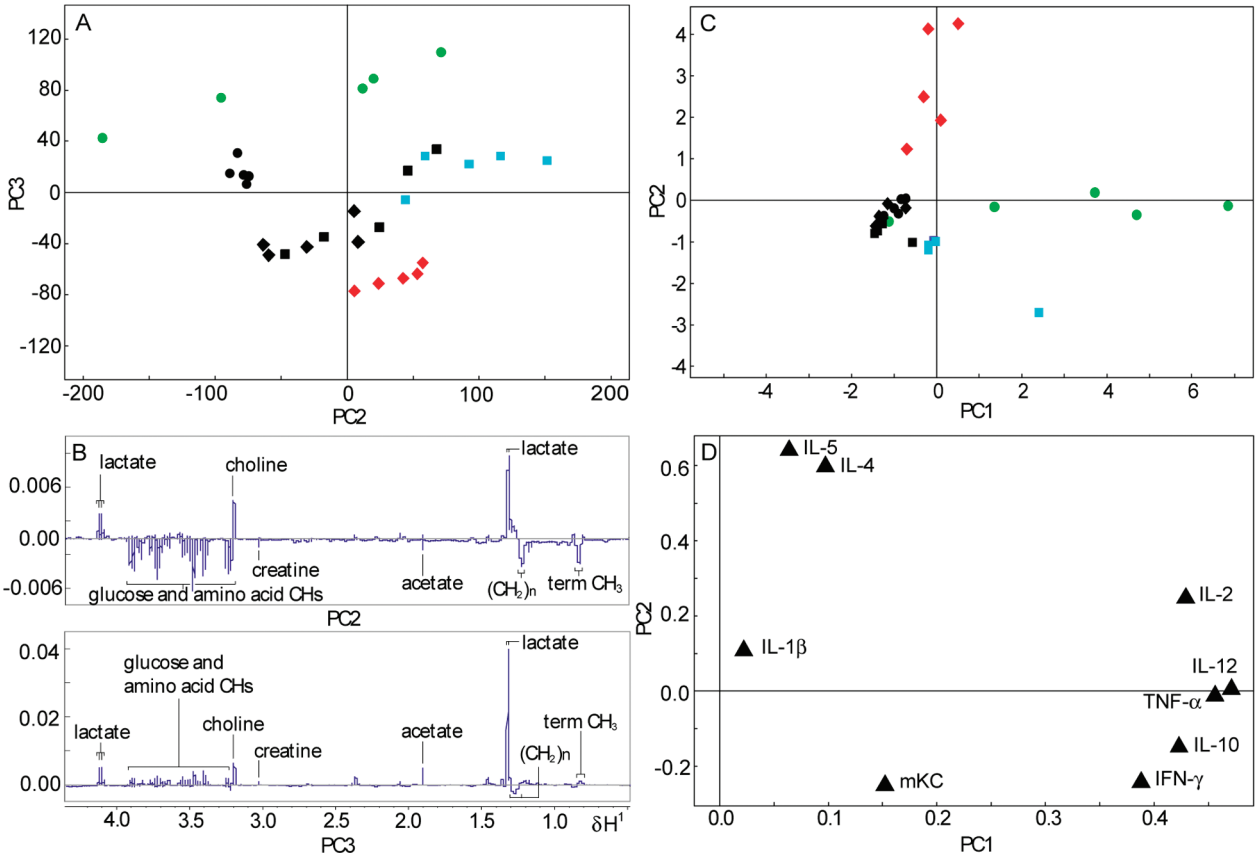

Figure 3. Global PLS-DA scores (A) and loadings line plots for discriminatory components 2 and 3 (B) from plasma ^{1}H NMR spectral data showing differentiation of the samples from noninfected control animals (black) and the 3 parasite-mouse models; *S. mansoni* (red), *T. b. brucei* (green), and *P. berghei* (blue). The protozoan infections are clearly differentiated from the noninfected and *S. mansoni*-infected groups along the first PC, while *S. mansoni* is differentiated from all other groups in the second PC. (C) PCA scores plot and (D) loadings plots derived from relative cytokine levels from matched animals from each infection model.

tokines were established, the correlations between the relative cytokine levels and metabolites were not significant, which may be due to the relatively small group sizes.

Discussion

Each of the assessed parasite−rodent models gave rise to a distinct pathological phenotype on the basis of both the metabolic and immunologic profiles.

Metabolic Phenotype Description of Parasite−Host Models. The metabolic fingerprint of each infection was composed of disease-specific features such as relatively increased urinary levels of pipecolic acid due to a *P. berghei* infection, or increased 4-hydroxyphenylacetic acid as response to a *T. b. brucei* infection (Table 1). On the other hand, several biomarkers were indicative of more than one infection, suggesting some commonly affected metabolic pathways across infections. Interestingly, many of the gut microbial-derived urinary metabolites seem to undergo similar directional changes in response to parasite infection, such as depleted concentrations of hippurate (*T. b. brucei*, *S. mansoni*, and *F. hepatica*), increased trimethylamine (*T. b. brucei* and *S. mansoni*) and increased phenylacetylglycine (*P. berghei* and *S. mansoni*). The association of hippurate, phenylacetylglycine, and the oxidized form of trimethylamine (TMAO) with gut microbial composition and/or activity has been underlined by studies on germ-free rats and mice with a reduced microbial composition.[40,41] The involvement of the gut microbiota has been discussed in more detail previously with regard to parasite infections.[2,3,30]

A common metabolic feature between *T. b. brucei* and *F. hepatica* was the elevation in levels of acetylated glycoproteins in plasma (both *N*- and *O*-acetyl glycoproteins). Acute phase proteins, such as transferrin, α-1-antitrypsin or haptoglobin, are secreted by hepatocytes in response to tissue damage and act as inflammatory mediators,[42,43] and thus, the increased concentrations of plasma acetylated glycoproteins are likely to reflect an inflammatory response.

Further analysis of *S. mansoni*-infected, noninfected control mice and the intermediate which group of 2 mice, which underwent experimental infection but which failed to establish adult worms, showed a comapping of the branched chain amino acids (BCAAs) with the established infection group, whereas the phenylacetylglycine, tyrosine and trimethylamine contributed most to the separation of the "intermediate" group, which may suggest an involvement of the gut microbial environment in susceptibility and resistance to a helminth infection and merits further investigation.

Comparison of the metabolic profiles of plasma across the three mouse models showed a spatial separation of the helminth infection from the two protozoan infections along the third PC. The corresponding loadings revealed relatively higher levels of lactate, acetate and creatine in the protozoan infections, whereas the $(CH_2)_n$-lipid signals were relatively lower.

Parasite Specific Differences in Cytokine Profiles. The cytokine modulations induced by each parasite were largely consistent with the literature.[6,44,45] The differentiation of

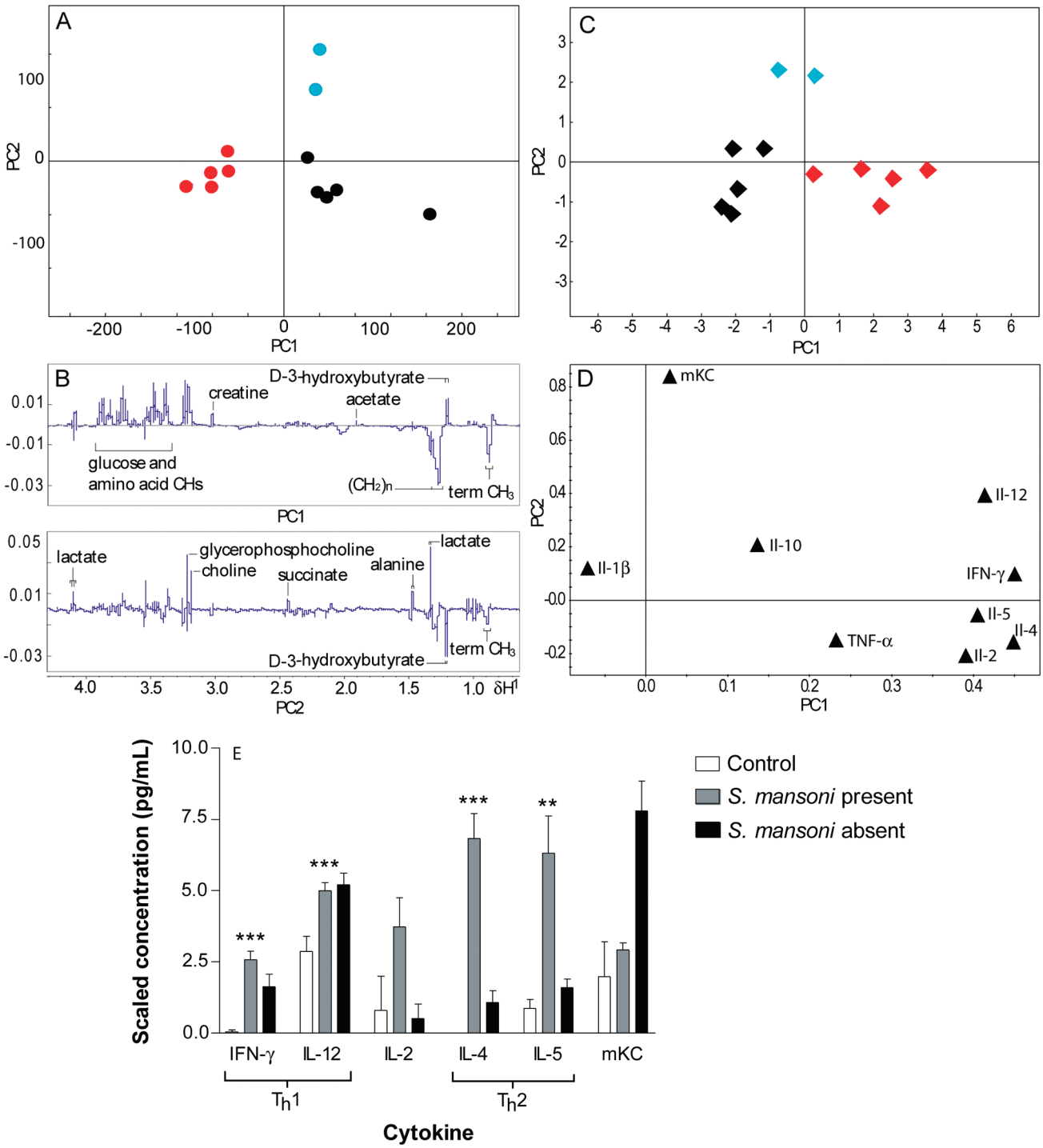

Figure 4. (A) PLS-DA scores plot showing plasma metabolite-based differentiation of *S. mansoni*-infected (red), noninfected control animals (black) and mice, which did not establish infection (possibly demonstrating early expulsion) as assessed upon dissection (blue), and (B) loadings line plot for the first and second PCs. (C) PCA scores plot of the relative plasma cytokine concentrations, and (D) main corresponding loadings showing similar infection-related clustering as the spectral data; (E) bar chart showing plasma cytokine concentrations for *S. mansoni*-infected mice. Values are mean ± standard deviation. Significance determined by Student's *t*-test (2-tailed, unpaired) p = * <0.05, ** <0.01, *** <0.001 (since there were only two animals in which infection failed to establish, statistical significance was not determined for the intermediate group). Note: Cytokine concentrations have been scaled to allow visual comparison across cytokines. IL-4 scaled 1:2, IL-5 scaled 1:10, IL-12 scaled 1:50 and mKC scaled 1:200. *No significance given for mKC for *S. mansoni*-absence since $n = 2$.

F. hepatica-infected from noninfected control rats was dominated by increased plasma IL-13, IL-5, and IL-1β levels (Table 1). IL-13, characteristically a Th2 cytokine, has been shown to directly inhibit pro-inflammatory cytokines in macrophages and plays an important role in minimizing the hepatic inflammation caused by the migrating larvae of *F. hepatica*. The cytokine response to the extracellular protozoan parasite *T. b. brucei* consisted of mixed Th-subset mechanisms reflecting both cell-mediated and humoral immune mechanisms. The main differential markers of infection with *P. berghei*, IL-12,

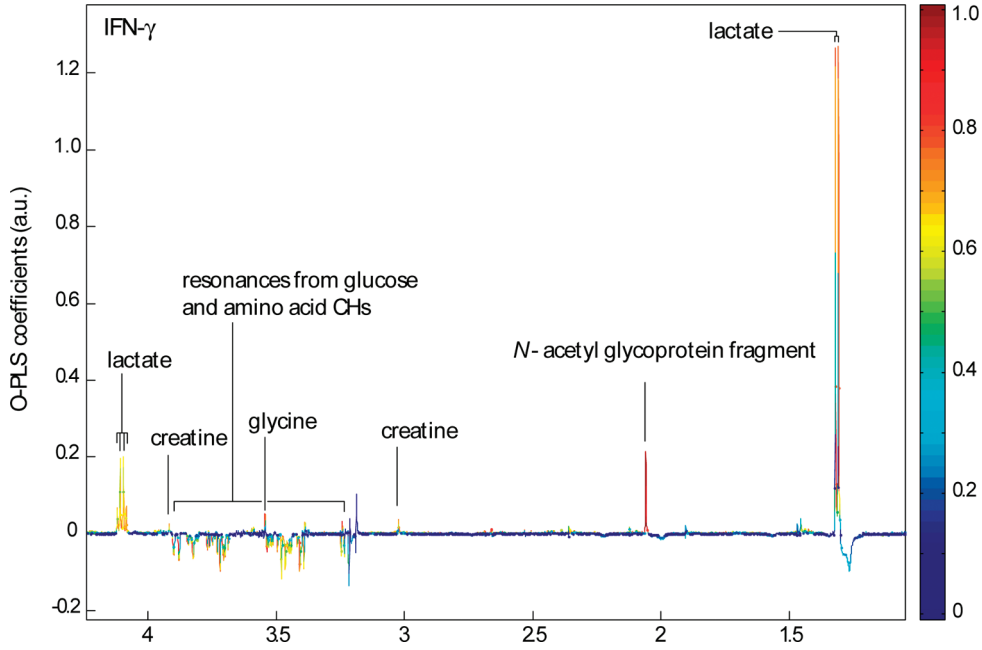

Figure 5. O-PLS correlation analysis of plasma obtained from *P. berghei*-infected mice ($n = 5$) before infection and on days 2 and 4 postinfection correlated with the individual matched relative levels of IFN-γ. Upward-oriented peaks represent positive correlation of metabolites with IFN-γ concentration and *vice versa.* a.u. denotes arbitrary unit.

and IFN-γ, are typical Th1 cytokines, whereas *S. mansoni* induced a Th2-dominated cytokine pattern (e.g., IL-4 and IL-5). As observed with the metabolic profiles, the *S. mansoni*-infected mice were further divided into two subgroups corresponding to 5 mice where infection was established as confirmed by worm counts in the liver and mesenteric veins[46] and 2 mice where infection failed to establish (intermediate group). The driving cytokine component in the intermediate group was mKC, whereas the main descriptors for established infection were the Th2 cytokines IL-4, IL-5, and IL-10. Although, the most effective response to a worm infection is believed to be Th2-based, *S. mansoni* seems more efficiently controlled by an initial strong cell-mediated (Th1) mechanism, which transfers to a Th2-mediated response with progressing course of disease in order to counteract the chronic inflammation caused by the eggs in the liver and other tissues.[45,47] The mouse functional analogue of human IL-8, mKC, has been shown to play a major role in acute inflammation by recruiting and activating neutrophils to the sites of inflammation,[48,49] which raises the question if those functions would be crucial to the expulsion of *S. mansoni* in particular.

Direct comparison of the plasma cytokine profiles from *S. mansoni* with those from both protozoan infections in a PCA analysis (Figure 3C) showed clustering of all corresponding control animals and separation of the three infected groups, wherein the 2 groups of mice infected by the protozoan parasites were differentiated from the controls in the first PC and from the trematode infection in the second component. However, the two protozoan infections could also be differentiated from each other with respect to the infection-induced alterations in host cytokine levels.

It is widely established that helminth infections induce a strong Th2-mediated immune response and here the *S. mansoni*-induced cytokine expression at a chronic stage time point was consistent with Th2-dominated immune mechanisms. The Th1 subset of cytokines involved in the response to *T. b. brucei* and *P. berghei*, on the other hand, was stronger, as suggested by increased IL-12 and IFN-γ, which are ranked higher in the list of the discriminatory cytokines in the protozoan infections, particularly with respect to *P. berghei*. Many protozoan parasites have intracellular stages where they are cleared by cell-mediated immune mechanisms induced by the Th1 cytokine subset.[6,26] Even though *T. b. brucei* is an extracellular parasite like *S. mansoni*, its effect on the host immune system is closer to that of *P. berghei*, which manifests both intra- and extracellular stages.

African trypanosome species trigger a strong cellular immune response (Th1-mediated) in infected mice *via* their variant surface glycoproteins (VSGs), which cover the parasite coat, and for which constant remodeling contributes to successful evasion from the humoral immunity.[50] The relatively lower plasma levels of triglycerides (VLDL/LDL) and phosphatidylcholine observed following a *T. b. brucei* infection, with subsequent increase of choline in the plasma of *T. b. brucei*-infected mice may be associated with the constant remodeling of the glycosylphosphatidylinositol (GPI) anchor of *T. b. brucei*, in order to enable the rapidly changing VSG composition. VSGs also induce secretion of TNF-α, which initiates B-cell proliferation and has a direct cytotoxic effect on *T. b. brucei*.[51]

Covariance between Metabolic and Cytokine Data. To obtain an overview of the global similarities/dissimilarities between the different infection-induced signatures of the 3 parasite-mouse models, comparison of the plasma (Figure 3) and urine samples (data not shown) was made. Both the metabolic and the cytokine data yielded a similar distribution of samples (Figure 3), in that samples of the protozoan infections were differentiated both from the control and from the helminth infection samples. A tight clustering of the cytokine data from all control samples was noted in the scores plot generated from the cytokine data. However, with respect to the metabolic data, batch differences between the control samples in both the urine (data not shown) and the plasma data sets were evident. This is unsurprising given that the NMRI mouse is an outbred strain and the ^{1}H NMR metabolic profiles

are composed of thousands of signals, which contribute to the model and which all have the potential to exhibit batch variation, whereas the cytokine panel represents a relatively coarse profile consisting of only 9 variables. Temporal and batch differences in ^{1}H NMR spectra of biofluids are well documented and result from the high sensitivity of the technology.[52,53] However, despite the observed batch-to-batch variation between the 3 parasite−mouse models, the parasite-induced alteration in the metabolic signature was stronger and the presence of these batch differences did not impede detection of clear infection-induced responses with further differentiation of the protozoan and helminth infections.

Analysis of each parasite−rodent model uncovered covariation between a range of metabolic and immune features, which may potentially be mechanistically related. In the correlation assessment of plasma ^{1}H NMR spectral data and cytokine concentrations in the *P. berghei* data set, direct statistical connections with biological coherence were evident, such as the positive correlations of IFN-γ, with *N*-acetyl glycoproteins, whereby both are important pro-inflammatory signaling molecules.

On the other hand, the positive correlation of IFN-γ with lactate and subsequent negative correlation with glucose deriving from the *P. berghei*-induced increase in the glycolytic activity may simply reflect the fact that these changes dominated the cytokine and metabolic profiles, respectively, and thereby the statistical correlation may result from covariation without necessarily inferring a direct mechanistic link. However, as all other assessed cytokines did not show any significant correlation with either glucose or lactate, a more direct involvement of the immune system and the components of the glycolysis may still be implicated.

To explore causality, with respect to the observed covariation, further studies are required. Focusing on the direct correlation of metabolic and immune components, this approach will ultimately allow the extraction of directly related events at the interface of metabolic and immune system and provide a mechanistic tool for probing pathology.

Conclusion

The approach employed in the current analysis, based on the parallel and integrated assessment of the metabolite and cytokine profiles from experimental infections in rodent models, enabled the extraction of the component of the metabolic signature directly and indirectly associated with immune mechanisms. A deeper understanding of the association between metabolic and immune events in these well-controlled laboratory models could open new avenues in understanding immunoregulatory mechanisms and their functions acting at a global metabolic level across a wide range of parasitic infections and diseases.

Acknowledgment. This work received financial support from Imperial College London, Biomedical Science Division and the Swiss National Science Foundation to J.S., J.V.L. and J.U. (project no. PPOOB-102883 and PPOOB-119129). Additional support was provided for J.S. by the Wellcome Trust/Imperial College VIP award (PS1041) and the Sir Henry Wellcome Fellowship (Wellcome Trust award number P23665).

Supporting Information Available: PCA of ^{1}H NMR spectra of plasma in *S. mansoni*-infected, noninfected control mice and two animals which were infected but where infection failed to establish during the course of the experiment; global PCA scores plot of plasma ^{1}H NMR spectral data of *S. mansoni*-infected, *T. b. brucei*-infected, *P. berghei*-infected and noninfected control mice; O-PLS-DA scores and corresponding loading plots derived from *T. b. brucei*−mouse. This material is available free of charge *via* the Internet at http://pubs.acs.org.

References

(1) Roth, E., Jr. *Plasmodium falciparum* carbohydrate metabolism: a connection between host cell and parasite *Blood Cells* **1990**, *16* (2−3), 453−60, Discussion 461−6.
(2) Wang, Y.; Holmes, E.; Nicholson, J. K.; Cloarec, O.; Chollet, J.; Tanner, M.; Singer, B. H.; Utzinger, J. Metabonomic investigations in mice infected with *Schistosoma mansoni*: an approach for biomarker identification. *Proc. Natl. Acad. Sci. U.S.A.* **2004**, *101* (34), 12676–81.
(3) Li, J. V.; Wang, Y.; Saric, J.; Nicholson, J. K.; Dirnhofer, S.; Singer, B. H.; Tanner, M.; Wittlin, S.; Holmes, E.; Utzinger, J. Global metabolic responses of NMRI mice to an experimental *Plasmodium berghei* infection. *J. Proteome Res.* **2008**, *7* (9), 3948–56.
(4) King, C. H.; Dangerfield-Cha, M. The unacknowledged impact of chronic schistosomiasis. *Chronic Illn.* **2008**, *4* (1), 65–79.
(5) Mackintosh, C. L.; Beeson, J. G.; Marsh, K. Clinical features and pathogenesis of severe malaria. *Trends Parasitol.* **2004**, *20* (12), 597–603.
(6) Noël, W.; Raes, G.; Hassanzadeh Ghassabeh, G.; De Baetselier, P.; Beschin, A. Alternatively activated macrophages during parasite infections. *Trends Parasitol.* **2004**, *20* (3), 126–33.
(7) Hotez, P. J.; Molyneux, D. H.; Fenwick, A.; Ottesen, E.; Ehrlich Sachs, S.; Sachs, J. D. Incorporating a rapid-impact package for neglected tropical diseases with programs for HIV/AIDS, tuberculosis, and malaria. *PLoS Med.* **2006**, *3* (5), e102.
(8) Amole, B. O.; Clarkson, A. B., Jr.; Shear, H. L. Pathogenesis of anemia in *Trypanosoma brucei*-infected mice. *Infect. Immun.* **1982**, *36* (3), 1060–8.
(9) Stoltzfus, R. J.; Chwaya, H. M.; Tielsch, J. M.; Schulze, K. J.; Albonico, M.; Savioli, L. Epidemiology of iron deficiency anemia in Zanzibari schoolchildren: the importance of hookworms. *Am. J. Clin. Nutr.* **1997**, *65* (1), 153–9.
(10) Anumudu, C.; Afolami, M.; Igwe, C.; Nwagwu, M.; Keshinro, O. Nutritional anaemia and malaria in preschool and school age children. *Ann. Afr. Med.* **2008**, *7* (1), 11–7.
(11) Saric, J.; Wang, Y.; Li, J.; Coen, M.; Utzinger, J.; Marchesi, J. R.; Keiser, J.; Veselkov, K.; Lindon, J. C.; Nicholson, J. K.; Holmes, E. Species variation in the fecal metabolome gives insight into differential gastrointestinal function. *J. Proteome Res.* **2008**, *7* (1), 352–60.
(12) Longfils, P.; Heang, U. K.; Soeng, H.; Sinuon, M. Weekly iron and folic acid supplementation as a tool to reduce anemia among primary school children in Cambodia. *Nutr. Rev.* **2005**, *63* (12 Pt. 2), S139–45.
(13) Alexander, J.; Bryson, K. T helper (h)1/Th2 and *Leishmania*: paradox rather than paradigm. *Immunol. Lett.* **2005**, *99* (1), 17–23.
(14) Peters, N.; Sacks, D. Immune privilege in sites of chronic infection: *Leishmania* and regulatory T cells. *Immunol. Rev.* **2006**, *213*, 159–79.
(15) Belkaid, Y.; Blank, R. B.; Suffia, I. Natural regulatory T cells and parasites: a common quest for host homeostasis. *Immunol. Rev.* **2006**, *212*, 287–300.
(16) Joosten, S. A.; Ottenhoff, T. H. Human CD4 and CD8 regulatory T cells in infectious diseases and vaccination. *Hum. Immunol.* **2008**, *69* (11), 760–70.
(17) Bettelli, E.; Korn, T.; Kuchroo, V. K. Th17: the third member of the effector T cell trilogy. *Curr. Opin. Immunol.* **2007**, *19* (6), 652–7.
(18) Mosmann, T. R.; Coffman, R. L. TH1 and TH2 cells: different patterns of lymphokine secretion lead to different functional properties. *Annu. Rev. Immunol.* **1989**, *7*, 145–73.
(19) Mosmann, T. R.; Sad, S. The expanding universe of T-cell subsets: Th1, Th2 and more. *Immunol. Today* **1996**, *17* (3), 138–46.
(20) Mosmann, T. R.; Cherwinski, H.; Bond, M. W.; Giedlin, M. A.; Coffman, R. L. Two types of murine helper T cell clone. I. Definition according to profiles of lymphokine activities and secreted proteins. *J. Immunol.* **1986**, *136* (7), 2348–57.
(21) Pearce, E. J.; Kane, C. M.; Sun, J.; Taylor, J. J.; McKee, A. S.; Cervi, L. Th2 response polarization during infection with the helminth parasite *Schistosoma mansoni*. *Immunol. Rev.* **2004**, *201*, 117–26.

(22) Hall, L. R.; Mehlotra, R. K.; Higgins, A. W.; Haxhiu, M. A.; Pearlman, E. An essential role for interleukin-5 and eosinophils in helminth-induced airway hyperresponsiveness. *Infect. Immun.* **1998**, *66* (9), 4425–30.
(23) Wilson, M. S.; Mentink-Kane, M. M.; Pesce, J. T.; Ramalingam, T. R.; Thompson, R.; Wynn, T. A. Immunopathology of schistosomiasis. *Immunol. Cell. Biol.* **2007**, *85* (2), 148–54.
(24) Korn, T.; Oukka, M.; Kuchroo, V.; Bettelli, E. Th17 cells: effector T cells with inflammatory properties. *Semin. Immunol.* **2007**, *19* (6), 362–71.
(25) Basso, A. S.; Cheroutre, H.; Mucida, D. More stories on Th17 cells. *Cell Res.* **2009**, *19* (4), 399–411.
(26) Jankovic, D.; Sher, A.; Yap, G. Th1/Th2 effector choice in parasitic infection: decision making by committee. *Curr. Opin. Immunol.* **2001**, *13* (4), 403–9.
(27) Keun, H. C.; Sidhu, J.; Pchejetski, D.; Lewis, J. S.; Marconell, H.; Patterson, M.; Bloom, S. R.; Amber, V.; Coombes, R. C.; Stebbing, J. Serum molecular signatures of weight change during early breast cancer chemotherapy. *Clin. Cancer Res.* **2009**, *15* (21), 6716–23.
(28) Martin, F. P. J.; Rezzi, S.; Philippe, D.; Tornier, L.; Messlik, A.; Hoelzlwimmer, G.; Bauer, P.; Quintanilla-Fend, L.; Loh, G.; Blaut, M.; Blum, S.; Kochhar, A.; Haller, D. Metabolic assessment of gradual development of moderate experimental colitis in IL-10 deficient mice. *J. Proteome Res.* **2009**, *8* (5), 2376–87.
(29) Grootveld, M.; Claxson, A. W. D.; Chaman, L. C.; Haycock, P.; Blake, D. R.; Haqwkes, G. E. High resolution proton NMR investigations of rat blood plasma. *FEBS.* **1993**, *322* (3), 266–276.
(30) Wang, Y.; Utzinger, J.; Saric, J.; Li, J. V.; Burckhardt, J.; Dirnhofer, S.; Nicholson, J. K.; Singer, B. H.; Brun, R.; Holmes, E. Global metabolic responses of mice to *Trypanosoma brucei brucei* infection. *Proc. Natl. Acad. Sci. U.S.A.* **2008**, *105* (16), 6127–32.
(31) Martins, Y. C.; Smith, M. J.; Pelajo-Machado, M.; Werneck, G. L.; Lenzi, H. L.; Daniel-Ribeiro, C. T.; Carvalho, L. J. Characterization of cerebral malaria in the outbred Swiss Webster mouse infected by *Plasmodium berghei* ANKA. *Int. J. Exp. Pathol.* **2009**, *90* (2), 119–30.
(32) Keita, M.; Bouteille, B.; Enanga, B.; Vallat, J. M.; Dumas, M. *Trypanosoma brucei brucei*: a long-term model of human African trypanosomiasis in mice, meningo-encephalitis, astrocytosis, and neurological disorders. *Exp. Parasitol.* **1997**, *85* (2), 183–92.
(33) el-Cheikh, M. C.; Borojevic, R. Extramedullar proliferation of eosinophil granulocytes in chronic schistosomiasis mansoni is mediated by a factor secreted by inflammatory macrophages. *Infect. Immun.* **1990**, *58* (3), 816–21.
(34) Murell, K. D., Fried, B. *Food-Borne Parasitic Zoonoses: Fish and Plant Borne Parasites*; Springer: New York, NY, 2007; Vol. 11.
(35) Chowdhury, F.; Williams, A.; Johnson, P. Validation and comparison of two multiplex technologies, Luminex and Mesoscale Discovery, for human cytokine profiling. *J. Immunol. Methods* **2009**, *340* (1), 55–64.
(36) Eriksson, L.; Antti, H.; Gottfries, J.; Holmes, E.; Johansson, E.; Lindgren, F.; Long, I.; Lundstedt, T.; Trygg, J.; Wold, S. Using chemometrics for navigating in the large data sets of genomics, proteomics, and metabonomics. *Anal. Bioanal. Chem.* **2004**, *380* (3), 419–29.
(37) Trygg, J.; Holmes, E.; Lundstedt, T. Chemometrics in metabonomics. *J. Proteome Res.* **2007**, *6* (2), 469–79.
(38) Trygg, J.; Wold, S. Orthogonal projections to latent structures (O-PLS). *J. Chemom.* **2002**, *16* (3), 119–128.
(39) Cloarec, O.; Dumas, M. E.; Trygg, J.; Craig, A.; Barton, R. H.; Lindon, J. C.; Nicholson, J. K.; Holmes, E. Evaluation of the orthogonal projection on latent structure model limitations caused by chemical shift variability and improved visualization of biomarker changes in ^{1}H NMR spectroscopic metabonomic studies. *Anal. Chem.* **2005**, *77* (2), 517–26.
(40) Nicholls, A. W.; Mortishire-Smith, R. J.; Nicholson, J. K. NMR spectroscopic-based metabonomic studies of urinary metabolite variation in acclimatizing germ-free rats. *Chem. Res. Toxicol.* **2003**, *16* (11), 1395–404.
(41) Yap, I. K. S.; Li, J. V.; Saric, J.; Martin, F. P.; Davies, H.; Wang, Y.; Wilson, I. D.; Nicholson, J. K.; Utzinger, J.; Marchesi, J. R.; Holmes, E. Metabonomic and microbiological analysis of the dynamic effect of vancomycin-induced gut microbiota modification in the mouse. *J. Proteome Res.* **2008**, *7* (9), 3718–28.
(42) Farinati, F.; Cardin, R.; De Maria, N.; Della Libera, G.; Marafin, C.; Lecis, E.; Burra, P.; Floreani, A.; Cecchetto, A.; Naccarato, R. Iron storage, lipid peroxidation and glutathione turnover in chronic anti-HCV positive hepatitis. *J. Hepatol.* **1995**, *22* (4), 449–56.
(43) Hervieu, V.; Lombard-Bohas, C.; Dumortier, J.; Boillot, O.; Scoazec, J. Y. Primary acinar cell carcinoma of the liver. *Virchows Arch.* **2008**, *452* (3), 337–41.
(44) Perlmann, P.; Perlmann, H.; Berzins, K.; Troye-Blomberg, M. Selected problems of malaria blood stage immunity. *Tokai J. Exp. Clin. Med.* **1998**, *23* (2), 55–62.
(45) Caldas, I. R.; Campi-Azevedo, A. C.; Oliveira, L. F.; Silveira, A. M.; Oliveira, R. C.; Gazzinelli, G. Human schistosomiasis mansoni: immune responses during acute and chronic phases of the infection. *Acta Trop.* **2008**, *108* (2−3), 109–17.
(46) Li, J. V.; Holmes, E.; Saric, J.; Keiser, J.; Dirnhofer, S.; Utzinger, J.; Wang, Y. Metabolic profiling of a *Schistosoma mansoni* infection in mouse tissues using magic angle spinning-nuclear magnetic resonance spectroscopy. *Int. J. Parasitol.* **2009**, *39*, 547–58.
(47) Pearce, E. J.; MacDonald, A. S. The immunobiology of schistosomiasis. *Nat. Rev. Immunol.* **2002**, *2* (7), 499–511.
(48) Ajuebor, M. N.; Das, A. M.; Virag, L.; Flower, R. J.; Szabo, C.; Perretti, M. Role of resident peritoneal macrophages and mast cells in chemokine production and neutrophil migration in acute inflammation: evidence for an inhibitory loop involving endogenous IL-10. *J. Immunol.* **1999**, *162* (3), 1685–91.
(49) Harada, A.; Sekido, N.; Akahoshi, T.; Wada, T.; Mukaida, N.; Matsushima, K. Essential involvement of interleukin-8 (IL-8) in acute inflammation. *J. Leukocyte Biol.* **1994**, *56* (5), 559–64.
(50) Donelson, J. E.; Hill, K. L.; El-Sayed, N. M. Multiple mechanisms of immune evasion by African trypanosomes. *Mol. Biochem. Parasitol.* **1998**, *91* (1), 51–66.
(51) Vincendeau, P.; Bouteille, B. Immunology and immunopathology of African trypanosomiasis. *An. Acad. Bras. Cienc.* **2006**, *78* (4), 645–65.
(52) Maher, A. D.; Zirah, S. F.; Holmes, E.; Nicholson, J. K. Experimental and analytical variation in human urine in ^{1}H NMR spectroscopy-based metabolic phenotyping studies. *Anal. Chem.* **2007**, *79* (14), 5204–11.
(53) Teahan, O.; Gamble, S.; Holmes, E.; Waxman, J.; Nicholson, J. K.; Bevan, C.; Keun, H. C. Impact of analytical bias in metabonomic studies of human blood serum and plasma. *Anal. Chem.* **2006**, *78* (13), 4307–18.

PR901019Z